Journal of The Electrochemical Society, **161** (5) D195-D201 (2014)
0013-4651/2014/161(5)/D195/7/$31.00 © The Electrochemical Society

Control of Nanostructure and Crystallographic Orientation in Electrodeposited ZnO Thin Films via Structure Directing Agents

Keigo Ichinose,[a] Tomoaki Mizuno,[a] Matthew Schuette White,[b] and Tsukasa Yoshida[c,z]

[a]*Graduate School of Engineering, Gifu University, Gifu 501-1193, Japan*
[b]*Linz Institute for Organic Solar Cells (LIOS), Physical Chemistry, Johannes Kepler University, A-4040 Linz, Austria*
[c]*Graduate School of Science and Engineering, Yamagata University, Yonezawa, Yamagata 992-8510, Japan*

The nanostructure and crystallographic orientation of ZnO thin films were controlled by using structure directing agents (SDAs) in the electrodeposition from O_2-saturated $ZnCl_2$ aqueous solutions. While hybrid thin film with eosin Y (ZnO_{EY}) has a nanoporous structure oriented with the *c*-axis in perpendicular to the substrate, that with citric acid (ZnO_{CA}) was found to have a contrasting lamellar structure consisting of stacked platelets of ZnO and oriented with its *c*-axis in parallel with the substrate. We show that switching of the SDA from CA to EY during the course of electrodeposition of a film changes the nanostructure but preserves crystal orientation. We propose a mechanism whereby the SDA can define crystallographic orientation from the randomly oriented seed layer. However once the orientation is defined, it is maintained by homoepitaxial growth of ZnO crystallites and the SDA will define only the morphology. This way, bilayer ZnO films with totally different crystallographic orientation but almost identical nanostructure were prepared. Dye-sensitized solar cells employing these films were used to investigate the influence of the *c*-axis orientation on the efficiency of electron injection recombination.

Manuscript submitted January 6, 2014; revised manuscript received February 21, 2014. Published March 5, 2014.

Zinc oxide (ZnO) has attracted a great deal of attention, with numerous applications such as UV light emitters,[2] varistors,[3,4] transducers,[5] transparent conducting electrodes,[6,7] sensors,[8] and catalysts.[9,10] The wide-bandgap semiconductor (bandgap of 3.3 eV and an excitonic binding energy of 60 meV)[1] is unique among metal oxides in that highly crystallized thin films can directly be obtained from aqueous solutions at low temperatures, owing to its relatively high chemical reactivity. In 1996, Izaki et al.,[11,12] and Peulon et al.[13,14] introduced electrodeposition of ZnO thin films from aqueous solution of zinc salts by electroreduction of nitrate ions and dissolved O_2, respectively. The film growth is simply achieved by surface reactions, namely, electron transfer for generation of OH^- and crystal growth of ZnO. Epitaxial electrodeposition of single crystal thin films of ZnO was made possible by employing single crystal conductive substrates with matched atomic geometry.[15–17] Furthermore, the crystal growth can be strongly influenced by the presence of surface adsorptive chemicals. For example, when eosin Y (abbreviated as EY, shown in scheme 1(a)) is added into the deposition bath as a structure directing agent (SDA), ZnO forms a highly crystallized nanoporous network. EY moleucles fill the pores, resulting in a self-assembled hybrid thin film.[18–22] The ZnO film hybridized with EY is oriented with its *c*-axis perpendicular to the substrate. On the other hand, addition of coumarin 343 (C343) yielded a porous ZnO made as an assembly of nano-sized platelets and oriented with its *c*-axis parallel to the substrate.[22]

The organic phase in the hybrid thin films can be totally removed by soaking the films into a medium to dissolve the organic molecules but not ZnO, such as dilute alkaline aqueous solution of pH 10 to 11. These "porous crystalline" ZnO films have high surface area and are free of grain boundaries, and are ideally suited as photoelectrodes in dye-sensitized solar cells (DSSCs), especially for flexible plastic substrates, because strongly adhesive and well conducting material can be obtained without high temperature annealing.[22] The great advantage of this process is also that fine tuning of the nanostructure as well as control of crystallographic orientation is made possible by simply changing the kind of SDA and deposition conditions, in order to further optimize the photoelectrode material to draw the best performance out of the photosensitizers and electrolytes to be combined. It is therefore worthwhile to explore possibilities for designing nanostructures employing various SDAs and is important to scrutinize the underlying mechanism for the structure control.

In this paper, EY and citric acid (abbreviated as CA, shown in scheme 1(b)) have been employed as SDAs for electrodeposition of hybrid thin films. CA is a typical chelating agent[23] having three carboxylic acid groups and has frequently been used as an SDA in the hydrothermal synthesis[24,25] and the chemical precipitation[26] of ZnO crystals. Hybridization with CA during the electrodeposition of ZnO resulted in a contrasting crystallographic orientation to that with EY, namely, to orient the *c*-axis in parallel with the substrate plane. Thus, CA behaves similarly to the previously reported C343 as a SDA.[22] Here we further investigate the effects of switching of the SDA from CA to EY during a film growth. Primarily, we test to see whether the orientation and nanostructure are preserved upon switching of the SDA. Our results indicate that the crystal orientation is fixed by the first layer and preserved throughout the growth, but that the nanostructure switches with the SDA. This provides us a unique opportuintiy to investigate the properties of multilayered nanoporous ZnO thin films as photoelectrodes in DSSC, with nearly idenital nanostrucures but orthogonal crystal orientation.

Experimental

F-doped SnO_2 (FTO) coated glass (Asahi glass, 10 Ω / sq.) used as the substrate was washed with detergent, pure water, acetone and 2-propanol. The FTO glass was mounted to a cylindrically shaped attachment with an insulating masking tape (Nitto Denko) with a 22 mm round hole in the center and attached to a commercial rotating disk electrode (RDE) system (AUTOLAB).[27] The FTO surface was soaked in a 45% HNO_3 solution for 2 min and rinsed with water before use.[28]

A single compartment cell was employed, being equipped with the FTO glass RDE as a working, an Ag/AgCl (+0.199 V vs. NHE at 25°C) as a reference, and a Pt (for Zn^{2+} free solution) or Zn (Zn^{2+} containing solution) wire as a counter electrode. The temperature of the cell was maintained at 70°C in a thermostat bath. A Hokuto Denko HSV-100 or an HZ-3000 was used for the potential control and the

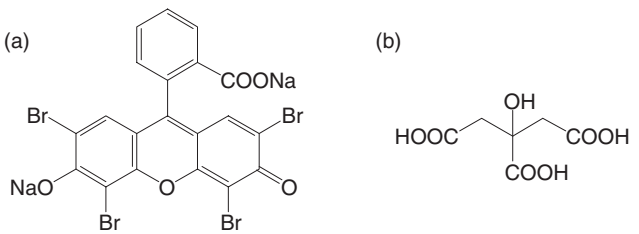

Scheme 1. Molecular structure of SDAs; (a) eosin Y (EY), (b) citric acid (CA).

[z]E-mail: yoshidat@yz.yamagata-u.ac.jp

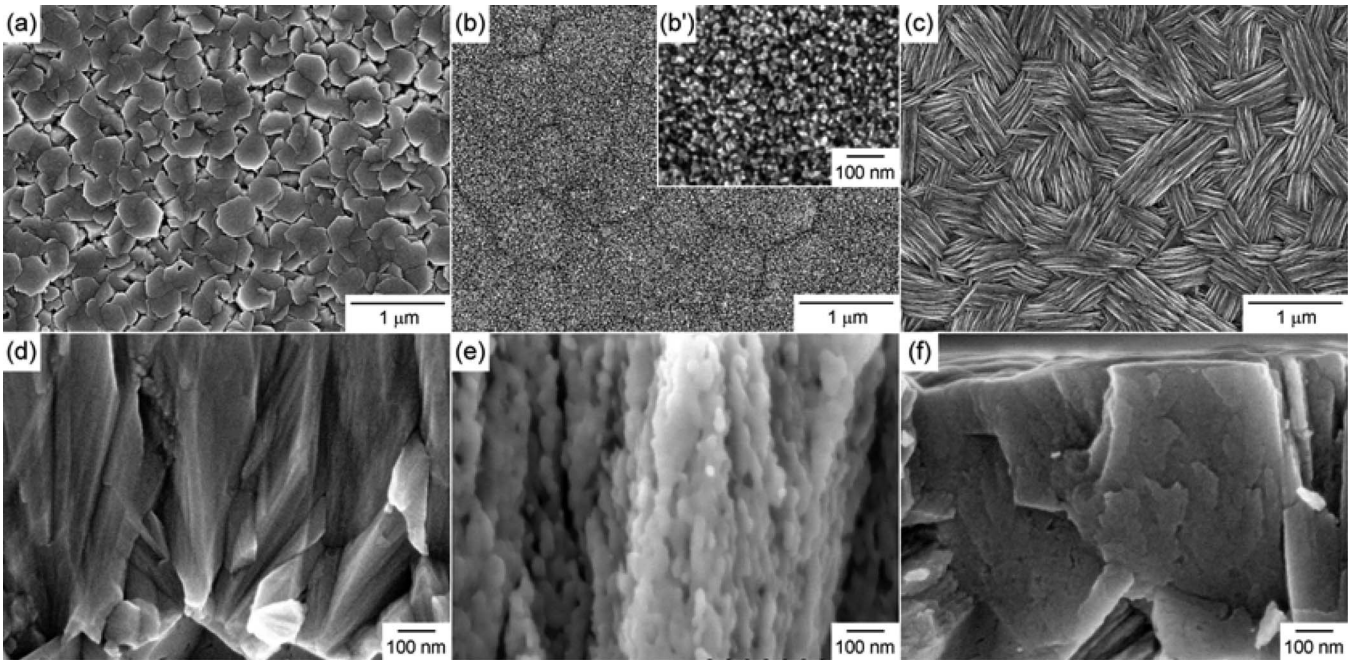

Figure 1. Surface and cross-sectional SEM pictures of electrodeposited (a, d) pure ZnO, (b, b′, e) ZnO_{EY} and (c, f) ZnO_{CA} thin films obtained after desorption of the loaded organic molecules.

current monitoring. The FTO glass electrode was activated toward O_2 reduction by electrolysis at −1.0 V and 500 rpm rotation speed for 30 min in an O_2 saturated 0.1 M KCl (Merck) aqueous solution.[27] Then, a small amount of concentrated $ZnCl_2$ (Merck) solution was added to the bath to achieve its concentration of 5 mM. Hybrid thin films with EY and CA were electrodeposited at −0.75 and −1.0 V from the baths containing 200 μM EY disodium salt (Kanto) and 10 μM CA monohydrate (Kishida), respectively. The electrodeposited hybrid thin films were soaked in a dilute KOH (Nacalai) aqueous solution (pH 10.5) for overnight to extract EY or CA molecules from the film.[22]

The surface and cross-sectional morphology of the films was observed on a Hitachi S-4300 or a JEOL JSM-6700F field emission scanning electron microscope (FE-SEM). X-ray diffraction (XRD) patterns of the films were measured on a Rigaku RINT-Ultima III/PC using Cu Kα radiation, in a shallow glazing angle (1.5°) 2θ-scan. The transmission absorption spectra of the films were measured on a Hitachi U-4000 double beam UV-vis spectrophotometer by taking a bare FTO glass as a reference.

ZnO thin films with 2.8 μm thickness of porous layer were sensitized at room temperature for 10 min in a 0.5 mM D149 (Mitsubishi Paper Mills) dye solution in an acetonirile/*tert*-buthyl alcohol (v/v = 1/1) mixture, also containing 1 mM cholic acid (Nacalai) to suppress dye aggregation.[29] The dyed ZnO electrode and a Pt-sputtered FTO glass counter electrode were assembled into a sandwich-type miniature cell (0.3 cm^2 area) using a hot-melt ionomer film as a spacer. An electrolyte solution consisting of 0.5 M tetrapropylammonium iodide (TPAI) and 0.05 M I_2 in an acetonitrile/ethylene carbonate (v/v = 1/4) mixture was loaded to the gap of the electrodes by capillary action. *I-V* curves of the cells were measured on an EKO MP-160 curve tracer under illumination with a simulated sun light (AM 1.5, 100 mW cm^{-2}) generated by a Yamashita-DensoYSS-150A. A mask was applied to the cells to regulate the active area to 0.2 cm^2 in this measurement.

Results and Discussion

Structures of ZnO hybrid thin films.— The electrodeposited ZnO thin film, and hybrid thin film with CA (denoted as ZnO_{CA}) were colorless, while that with EY (denoted as ZnO_{EY}) was red, adopting the color of the SDA. Surface and cross-section images of pure ZnO, ZnO_{EY} and ZnO_{CA} hybrid thin films after desorption of the loaded organic molecules are shown in Fig. 1. The pure ZnO thin films are made of hexagonal columnar grains which are typical for ZnO (Fig. 1a). The surface of the grains is smooth and each grain appears to be dense and monolithic. Tiny nanoparticles are visible on the surface of the ZnO_{EY} hybrid thin film (Fig. 1b, b′), which in fact is an observation of the oriented nanoporous structure visible in the cross section (Fig. 1e). The nanoporous ZnO is interconnected as a single crystal, which in turn can also be understood as such that vertically oriented pores occupy volume within a single crystal grain of ZnO.[22] By contrast, when CA was added to the bath, unique lamellar structure is seen on the surface (Fig. 1c), corresponding to the exposure of the edges of oriented and stacked platelets as seen in the cross section image (Fig. 1f).

The crystallographic orientation of these ZnO thin films was studied by XRD (Fig. 2). In case of the pure ZnO thin film, all major diffraction peaks are observed. The peak intensity from the (002) planes is relatively higher than that of the powder diffraction standard (bottom of Fig. 2), so that the crystallites have a tendency to be self-oriented with their *c*-axis being perpendicular with the substrate plane. Such preference is often observed because the (002) crystal face is the densest and thermodynamically most stable. A much stronger preference for the same *c*-axis orientation is observed for the ZnO_{EY} hybrid thin film (Fig. 2b). All diffraction peaks other than that from (002) disappear, except for the very small peak arising from the (103) planes, which are nearly parallel with (002). It is evident that EY brings about strong preference to orient the *c*-axis perpendicular to the substrate. A clearly contrasting pattern is obtained for the ZnO_{CA} hybrid thin film (Fig. 2c), exhibiting clearly enhanced peaks from the (100) and (110) planes compared to the others. Both of these planes are in parallel with the *c*-axis, indicating that the orientation is changed by 90° from that of the ZnO_{EY} to lay down the *c*-axis. The diffraction peak from the (002) planes in fact disappears for this sample. It is interesting to note that Azaceta et al.[30] and Tulodziecki et al.[31] reported formation of ZnO thin film oriented along the non-polar directions same as the ZnO_{CA} film in this study, by electrodeposition from oxygen-dissolved ionic liquid electrolyte. When nitrate ion was employed as oxide ion precursor in the same ionic liquid, they obtained ZnO thin

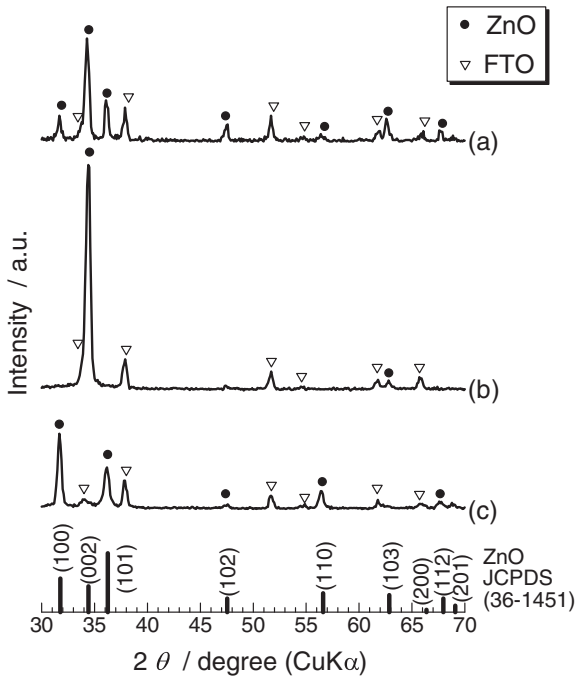

Figure 2. XRD 2θ-scan patterns of (a) pure ZnO, (b) ZnO_{EY}, and (c) ZnO_{CA} thin films electrodeposited on FTO glass substrates.

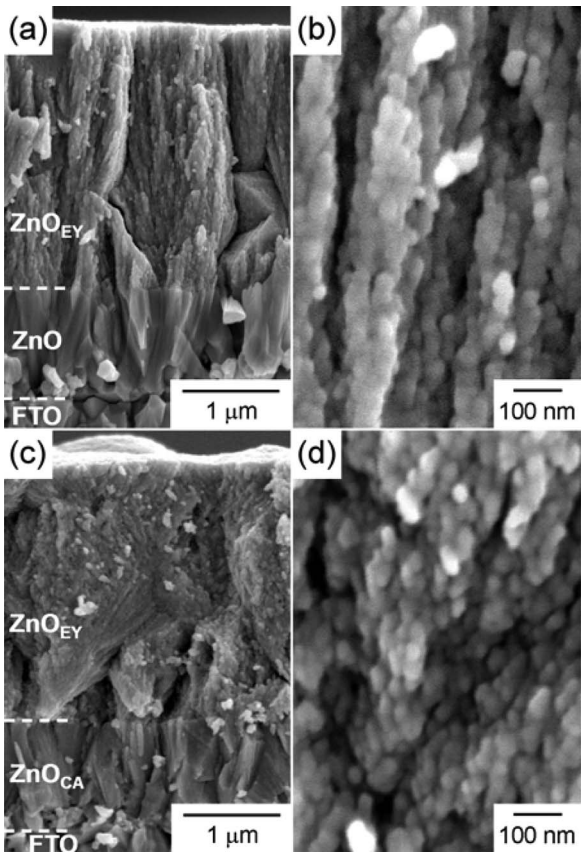

Figure 3. Cross-sectional SEM images of electrodeposited (a, b) ZnO/ZnO_{EY} and (c, d) ZnO_{CA}/ZnO_{EY} bilayers, where (b) and (d) correspond to the close-up of the ZnO_{EY} outer layer to show their nanostructures, respectively.

films in a conventional orientation, namely, *c*-axis perpendicular to the substrate.[32] The influence of CA was studied by varying its concentration, and even a minor addition at 2 μM was sufficient to cause the observed orientation change, while 20 μM was already too high thus hindering the formation of ZnO, due to much stronger coordination of CA to Zn^{2+} than that of EY (see supporting information Fig. 1S). On the other hand, CA did not show any catalytic activity to the reduction of O_2, by contrast to EY that enhances the O_2 reduction current and thus promotes formation of ZnO.[21] too.

Switching of SDA during the electrodeposition.— CA and EY were found to produce both different nanostructures and crystallographic orientation during growth of ZnO. Therefore, it is interesting to switch the SDA in the course of electrodeposition to check how the orientation and nano morphology change correspondingly. We have simply transferred the working electrode with already electrodeposited ZnO (*c*-axis perpendicular to the substrate) or ZnO_{CA} (*c*-axis parallel with the substrate) thin films to another cell containing the electrolyte with EY to deposit ZnO_{EY} layer on top of them. A set of results for such bilayer systems is shown in Fig. 3. The sharp border between the two layers is recognized for both samples because of abrupt change of nano morphologies. However, close up of the border (See supporting information Fig. 2S for the SEM picture) revealed seamless connection of the two layers. The same nanoporous structure of the ZnO_{EY} layer is seen for both samples, vertically aligned for that on ZnO, while being tilted for that on ZnO_{CA}. Interestingly, nano morphologies of these ZnO_{EY} layers are nearly identical, as seen in close up images of the cross section (Fig. 3b, 3d), looking like chains of interconnected particles of a few tens nm size. Despite of their similar morphologies, a remarkable difference was found in their XRD patterns (Fig. 4). Care was taken to reduce the signal from the bottom layer by placing the sample slightly below the plane of the sample holder for the XRD measurement. While the ZnO_{EY} layer on ZnO shows a strong (002) diffraction, the same hybrid layer on ZnO_{CA} exhibits clearly enhanced (100), (110) peaks and small one from (002), thus showing the same trends as those of the bottom layers. It is evident that the orientation of the ZnO_{EY} overlayer is preserved from the bottom layers. These results clearly indicate that SDAs are unable to change the crystallographic orientation once a ZnO layer with a certain orientation is present. It is understood that homoepitaxial growth of ZnO strongly operates and overrides the influence of the SDA. Because electrodeposition of ZnO is a typical atom-by-atom process in which the film growth is achieved by crystal growth, no new crystal grains are formed in the course of the electrodeposition, so that changing crystallographic orientation during the electrodeposition is virtually impossible. On the other hand, the nanostructure of the hybrid films reflects the influence of the SDA and it is not affected by the crystal orientation. Consequently, ZnO_{EY} layers with similar nanostructures but with totally different crystallographic orientations could be obtained by employing the bottom layers with different orientations.typical.

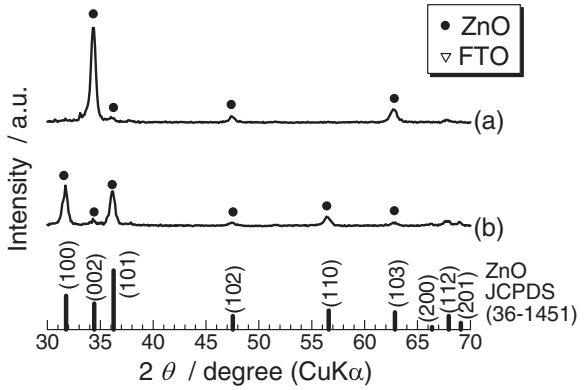

Figure 4. XRD 2θ-scan patterns of electrodeposited (a) ZnO/ZnO_{EY} and (b) ZnO_{CA}/ZnO_{EY} bilayers.

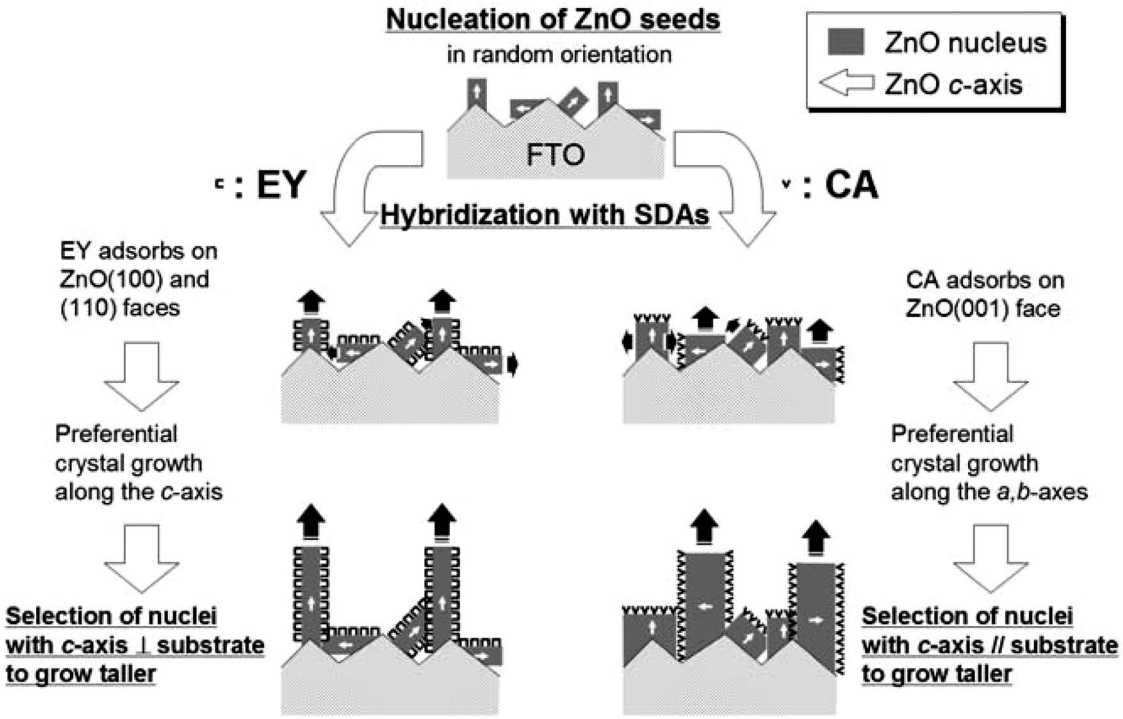

Figure 5. Illustration of the mechanism that cause different crystallographic orientations of the ZnO hybrid thin films with EY and CA, based on the selection of preferentially growing ZnO nuclei.

It is then important to discuss the origin of the orientation control by the SDA observed when the electrodeposition was carried out on a bare FTO glass electrode. The vertically aligned nanostructure and the direction of the *c*-axis are aligned in the ZnO_{EY} hybrid film deposited on FTO. It is supposed that EY molecules are preferentially adsorbed onto ZnO crystal faces parallel with the *c*-axis such as (100) and (110) to cause anisotropy in crystal growth to yield such oriented nanowires.[18] On the other hand, CA molecules are adsorbed preferentially onto the (002) planes of ZnO to suppress the crystal growth of ZnO along the *c*-axis, which in return favors the growth along the *a,b*-axes to yield stacks of ZnO platelets. The same mechanism has been discussed when coumarin 343[22] and 2,9,11,23-tetrasulfophthalocyaninato-dihydroxosilicon(IV)[33] were used as the SDA, yielding similar lamellar structure oriented in the *c*-axis in parallel with the substrate.

Since the FTO glass substrate used in this study is made of randomly oriented crystal grains of SnO_2, the ZnO nuclei produced right at the beginning of the electrolysis should also be randomly oriented. Selection of the nuclei then occurs in the subsequent process of crystal growth depending on the choice of the SDA. In the presence of EY, the crystal growth along the *c*-axis is preferred, so that the growth of the nuclei oriented with the *c*-axis perpendicular to the substrate prevails. The otherwise-oriented nucleation sites quickly stop their growth as they are buried underneath the preferentially grown grains. Consequently, the ZnO_{EY} hybrid on FTO tends to show the observed preferential orientation as the film grows thicker. Likewise, the addition of CA selects the nuclei oriented with their *c*-axis in parallel with the substrate to grow taller than the others, so that the ZnO_{CA} hybrid thin film becomes oriented with the flat laid *c*-axis. Such a mechanism for the control of the crystallographic orientation based on the selection of the nuclei by the SDA is illustrated in Fig. 5.

The corresponding mechanism for crystal growth upon switching the SDA is shown in Fig. 6. Hybridization with the SDA molecules causes anisotropy in crystal growth and development of nanostructures. However, the SDA molecules are unable to change the crystallographic orientation of the film because homoepitaxial growth of ZnO crystal continues to occur. As a consequence, porous ZnO_{EY} layers with totally different crystallographic orientation but with the same nano morphologies were obtained by employing the initially deposited ZnO layers with different orientations.

Optical properties of ZnO and ZnO_{CA} thin films.— The optical transmission curves were measured on ca. 1 μm thick pure ZnO and ZnO_{CA} thin films (Fig. 7A 7a and 7b). The transmittance exceeds 100% in the visible wavelength range, because the FTO glass sample used as the reference is hazy due to textured FTO layer. Deposition of ZnO flattens the surface to reduce the light scattering. Sharp decrease of transmission in the UV range is caused by bandgap absorption of ZnO. Interestingly, the onset for these two samples are clearly different, being shorter wavelength (higher energy) for ZnO_{CA} than ZnO. When these films are annealed at 300°C in air, their absorption onsets are red-shifted and fall onto almost the same wavelength (Fig. 7A(a′) and (b′)). Bandgap energy (E_g) of direct transition for these ZnO samples were estimated from the $(\alpha h\nu)^2$ vs. $h\nu$ plots (Fig. 7B). E_g of the as-deposited ZnO and ZnO_{CA} were 3.52 and 3.60 eV, while they were reduced to 3.30 and 3.32 eV after annealing, respectively. The E_g values after annealing are typically expected for bulk ZnO, whereas those of the as-deposited samples are unusually large. The E_g of the ZnO_{EY} hybrid thin film was similar to that of the pure ZnO. Such clear widening of the bandgap for electrodeposited ZnO and reduction to ca. 3.3 eV have also been reported by Pauporté et al.[28,34] The annealing of these samples did not cause any noticeable changes in their XRD patterns (not shown). It also did not change the morphologies of the films. The as-deposited samples are already well crystallized, so that the change of E_g cannot be associated with the ripening of ZnO crystals by heating. Since electrodeposition of ZnO is carried out under reductive conditions in water, oxygen defects and/or doping of interstitial atomic hydrogen are naturally expected, both of them acting as electron donors. Rather high donor density has indeed been found for electrodeposited ZnO nanowires.[35] Excessively high carrier density partially filling up the conduction band results in an increased threshold photon energy needed for electron transition from the valence band, known as Burstein-Moss effect.[36,37] The observed enlargement of E_g for the as-deposited films could be explained by

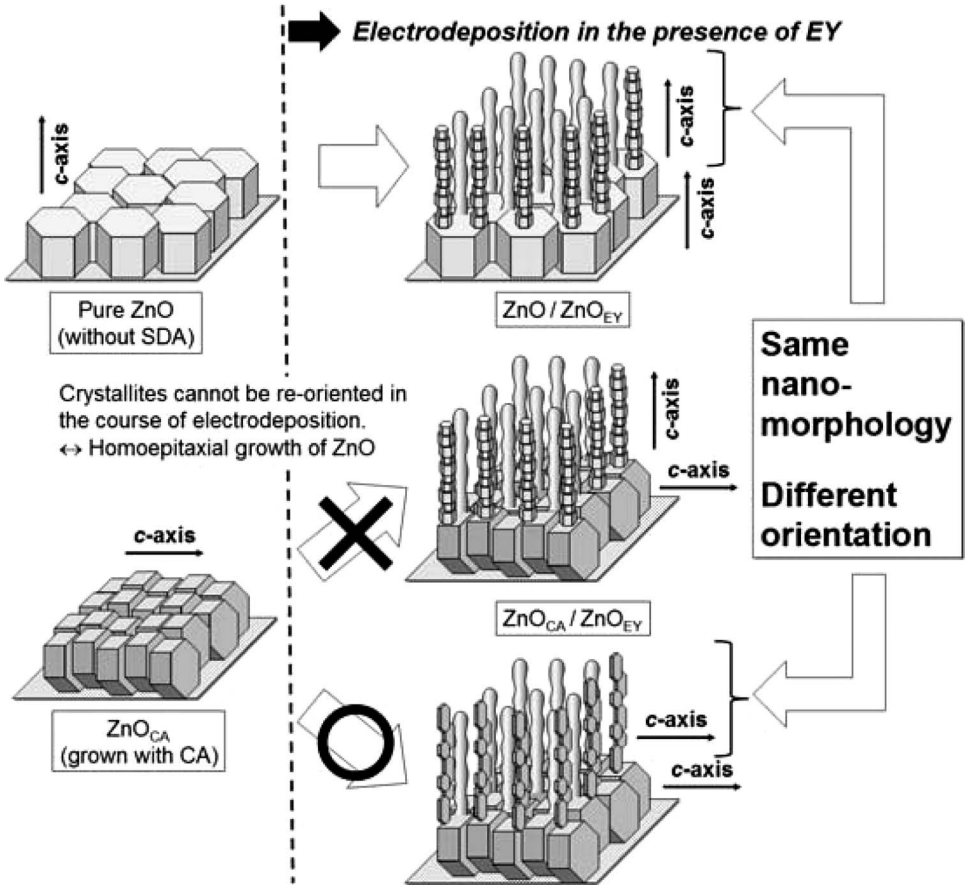

Figure 6. Illustration of the bilayer electrodeposition by switching SDAs in the course of the electrodeposition of ZnO.

such extremely high density of donors which are then undoped by the annealing to recover the typical E_g for bulk ZnO. The even larger E_g for ZnO_{CA} than pure ZnO and ZnO_{EY} could be associated with its even higher donor density, although they all go down to the same level after annealing.energy

Photoelectrode properties of differently oriented ZnO_{EY} films in DSSCs.— Since ZnO_{EY} porous films with similar nano morphologies but with different crystallographic orientations could be obtained by employing differently oriented bottom layers with and without CA, it is interesting to study their differences in photoelectrochemical properties in DSSCs. DSSCs employing bilayers of ZnO/ZnO_{EY} and ZnO_{CA}/ZnO_{EY} sensitized by D149 were fabricated and their *I-V* curves and cell properties are shown in Fig. 8 and Table I, respectively. The photocurrent of ZnO_{CA}/ZnO_{EY} cell is lower than that of ZnO/ZnO_{EY}, while the voltage is somewhat higher. Since the *F.F.* of the ZnO_{CA}/ZnO_{EY} cell is also lower, the overall conversion efficiency is lower (3.9%) than that of the ZnO/ZnO_{EY} cell (4.8%).

The difference of the photocurrent cannot be explained by that of the light harvesting efficiency, because their dye loading capability was similar as naturally expected from their similar nano morphology, thus the surface area. For both electrodes, the light absorption practically reaches its saturation around the absorption maximum of D149 for the porous layer with the thickness of 2.8 μm. Nonomura et al. have previously investigated the difference of the photoelectrochemical properties of differently oriented ZnO_{EY} and ZnO_{C343} layers, sensitized either with EY or C343, by photocurrent transient measurements and intensity modulated photocurrent and photovoltage spectroscopies (IMPS and IMVS).[38] Interestingly, it turned out that the electron diffusion in the ZnO_{C343} layer occurred much faster than in the ZnO_{EY}, as the electron mobility along the *a,b*-axes is known to be higher than that along the *c*-axis due to the anisotropic structure of ZnO,[39] even though the absolute magnitude of photocurrent was smaller for the ZnO_{C343}. Because of the difference not only for the crystal orientation but also the nanostructure and surface area, between ZnO_{EY} and ZnO_{C343} used in their study, the reason for the different photocurrent was obscured. Based on fitting of a theoretical model to the IMPS data, they extracted the quantum efficiencies for electron injection from dye excited states and found clearly smaller values for ZnO_{C343} than ZnO_{EY}, when the same sensitizer was used, even though both EY and C343 are not such good sensitizers and their absorption coefficients had to be underestimated to obtain reasonable fits. In the present study, the difference can be understood in a more straightforward manner, because the efficiency of light absorption is almost the same for ZnO/ZnO_{EY} and ZnO_{CA}/ZnO_{EY} bilayers sensitized with D149, and D149 is usually a good sensitizer for ZnO to achieve over 80% IPCE (incident photon to current conversion efficiency).[29] Reduced electron injection efficiency from D149 adsorbed to the ZnO_{CA}/ZnO_{EY} should therefore be responsible to the reduced photocurrent. Mainly exposed internala surface is of expectedly different crystal faces between ZnO/ZnO_{EY} and ZnO_{CA}/ZnO_{EY} due to their different crystal orientations and the same nanowire structure. It is then reasonable to expect different efficiencies for electron injection for sensitizer dye molecules attached to different crystal faces.

On the other hand, the cell employing the ZnO_{CA}/ZnO_{EY} electrode exhibited an open circuit voltage 30 mV higher than that of the ZnO/ZnO_{EY} cell. Increased voltage has also been reported by Nonomura et al. for the ZnO_{C343} electrode having the same orientation as the ZnO_{CA}/ZnO_{EY}.[38] The ZnO_{CA}/ZnO_{EY} cell also shows suppressed dark current compared to that of the ZnO/ZnO_{EY} cell. In order to gain further insights, Tafel plots were generated from the *I-V* curves close to the current onset for the I^-/I_3^- redox reactions measured for the ZnO and ZnO_{CA} bottom layers without the ZnO_{EY} porous

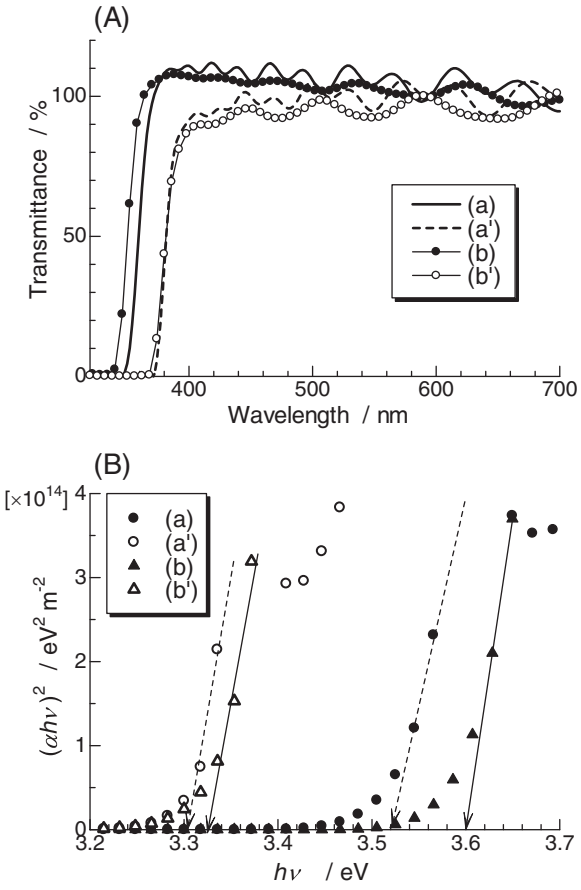

Figure 7. (A) Transmission spectra of as-electrodeposited (a) ZnO and (b) ZnO_{CA} thin films of ca. 1 μm thickness. (a′) and (b′) are those of the same films after annealing them at 300°C in air for 1 hour, respectively. (B) $(\alpha h\nu)^2$ vs. $h\nu$ plots calculated from the spectra shown in (A). The bandgap energy (E_g) was determined as (a) 3.52, (b) 3.60, (a′) 3.30, and (b′) 3.32 eV.

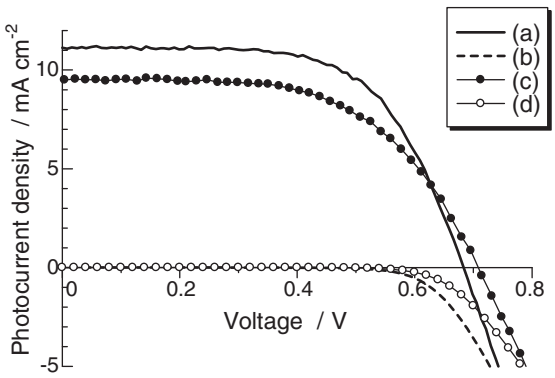

Figure 8. *I-V* curves of DSSCs employing (a, b) ZnO/ZnO_{EY} and (c, d) ZnO_{CA}/ZnO_{EY} bilayer photoelectrodes sensitized with D149 measured under illumination with (a, c) an AM 1.5 stimulated sunlight (100 mW cm^{-2}) and (b, d) in the dark.

Table I. Properties of DSSCs employing (a) ZnO/ZnO_{EY} and (b) ZnO_{CA}/ZnO_{EY} bilayer photoelectrodes sensitized with D149.

	*J*sc / mA cm^{-2}	*V*oc / V	*F.F.*	η / %
(a)	11.1	0.68	0.63	4.8
(b)	9.5	0.71	0.58	3.9

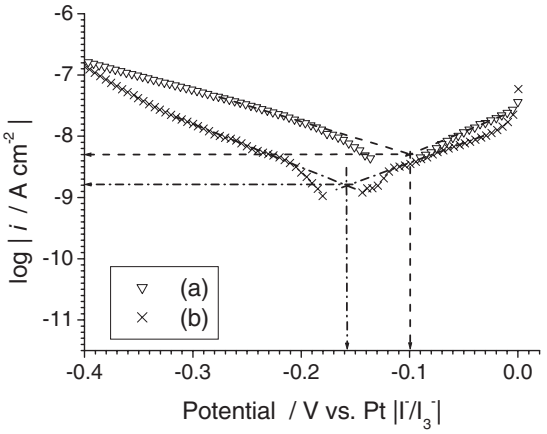

Figure 9. Tafel plots of *I-V* curves measured at (a) ZnO and (b) ZnO_{CA} electrodes in I/I_3^- redox electrolyte.

layer and without dye (Fig. 9). Potentials are referred to a Pt wire quasi-reference electrode whose potential is determined by that of the electrolyte. If there is no specific chemical interaction between ZnO electrodes and the iodide redox system, the equilibrium potential (E_{eq}) measured at the ZnO electrode should equal to that of the Pt reference, and that was not the case here. The E_{eq} of ZnO electrodes appeared more negative than that of the Pt reference. That of the ZnO electrode appeared at −0.10 V vs. Pt as determined from the Tafel plot, and it was further negatively shifted to −0.16 V vs. Pt for the ZnO_{CA}. Such a difference may be caused by the different doping levels of these films to bring about different structures of the electrochemical bilayers at the electrode/electrolyte interface. Exchange current densities for the ZnO and ZnO_{CA} films were determined as 5.0×10^{-9} and 1.6×10^{-9} A cm^{-2}, respectively. The suppressed recombination at the ZnO_{CA} bottom layer as well as the negative shift of E_{eq} thus explain the increased voltage for the ZnO_{CA}/ZnO_{EY} cell.

Conclusions

Control of nanostructure and crystallographic orientation by use of different SDAs in electrodeposition of ZnO thin films has been investigated. EY and CA were found to exhibit contrasting effects to cause anisotropy in the crystal growth resulting in characteristic nano morphologies and changes in preferential crystallographic orientation of the films. Experiments to switch the SDAs during deposition revealed that the SDAs are unable to change the crystallographic orientation but change the nanostructure. Because homoepitaxial growth of ZnO crystallites strongly operates even in the presence of the SDAs due to atom-by-atom growth character of ZnO electrodeposition. The crystallites cannot be re-oriented in the course of the film deposition. The origin of the orientation control by using SDAs and randomly structured substrate was understood as based on the selection of ZnO nuclei to grow preferentially because of the anisotropy of crystal growth imposed by the SDA molecules.

Combination of these strategies thus allowed us to prepare porous ZnO films with different orientation but with nearly identical nanostructures. As an example, the use of ZnO_{CA}/ZnO_{EY} bilayer oriented with the *c*-axis in parallel with the substrate in comparison to the traditionally used ZnO/ZnO_{EY} whose *c*-axis is in perpendicular with the substrate as photoelectrodes in DSSCs revealed increased voltage and decreased photocurrent. This method opens the possibilities to tune. almost independently, nanostructures, energetic structure and crystallographic orientation. Furthermore, it has been shown that such control does influence the device performance when employing such materials. Given the wide variety of SDAs available, we anticipate further exploration to enhance the usefulness of the electrochemical synthesis not only for DSSCs but also for various other applications of ZnO based materials.

Acknowledgments

This work was financially supported by the next generation PV R&D project of the New Energy and Industrial Technology Development Organization (NEDO) of Japan and grant-in-Aid for Scientific Research B (24350103) from the Ministry of Education, Sports and Culture of Japan (MEXT). We gratefully acknowledge Professor Niyazi Serdar Sariciftci for facilitating this collaboration between ROEL in Japan and LIOS in Austria in the framework of Japan Regional Innovation Strategy Program by the Excellence from JST, Japan.

References

1. J. M. Hvam, *Solid State Commun.*, **26**, 987 (1987).
2. A. Tsukazaki, M. Kubota, A. Ohtomo, T. Onuma, K. Ohtani, H. Ohno, S. F. Chichibu, and M. Kawasaki, *Jpn. J. Appl. Phys.*, **44**, L643 (2005).
3. D. Fernandez-Hevia, J. de Frutos, A. C. Caballero, and J. F. Fernandez, *Appl. Phys. Lett.*, **83**, 2692 (2003).
4. N. Ohashi, K. Kataoka, T. Ohgaki, T. Miyagi, H. Haneda, and K. Morinaga, *Appl. Phys. Lett.*, **83**, 4857 (2003).
5. Y. Hsu, J. Lin, and W. C. Tang, *J. Mater. Sci.*, **19**, 653 (2008).
6. M. Hiramatsu, K. Imaeda, N. Horio, and M. Nawata, *J. Vac. Sci. Technol. A*, **16**, 669 (1998).
7. H. Kim, C. M. Cilmore, J. S. Horwitz, A. Piqué, H. Murata, G. P. Kushto, R. Schlaf, Z. H. Kafafi, and D. B. Chrisey, *Appl. Phys. Lett.*, **76**, 259 (2000).
8. P. Mitra, A. P. Chatterjee, and H. S. Maiti, *J. Mater. Sci.: Mater. in Electronics*, **9**, 441 (1998).
9. H. Jacobs, W. Mokwa, D. Kohl, and G. Heiland, *Surf. Sci.*, **160**, 217 (1985).
10. C. T. Campbell, K. A. Daube, and J. M. White, *Surf, Sci.*, **182**, 458 (1987).
11. M. Izaki and T. Omi, *Appl. Phys. Lett.*, **68**, 2439 (1996).
12. M. Izaki and T. Omi, *J. Electrochem. Soc.*, **143**, L53 (1996).
13. S. Peulon and D. Lincot, *Adv. Mater.*, **8**, 166 (1996).
14. S. Peulon and D. Lincot, *J. Electrochem. Soc.*, **145**, 864 (1998).
15. T. Pauporté and D. Lincot, *Appl. Phys. Lett.*, **75**, 3817 (1999).
16. T. Pauporté, R. Cortes, M. Froment, B. Beaumont, and D. Lincot, *Chem. Mater.*, **14**, 4702 (2002).
17. K. Ichinose and T. Yoshida, *Phys. Stat. Sol. (a)*, **205**, 2376 (2008).
18. T. Yoshida, T. Pauporté, D. Lincot, T. Oekermann, and H. Minoura, *J. Electrochem. Soc.*, **150**, C608 (2003).
19. T. Pauporté, T. Yoshida, R. Cortès, M. Froment, and D. Lincot, *J. Phys. Chem. B*, **107**, 10077 (2003).
20. A. Goux, T. Pauporté, T. Yoshida, and D. Lincot, *Langmuir*, **22**, 10545 (2006).
21. D. Komatsu, J. Zhang, T. Yoshida, and H. Minoura, *Transactions of the Mater. Res. Soc. of Jpn.*, **32**, 417 (2007).
22. T. Yoshida, J. Zhang, D. Komatsu, S. Sawatani, H. Minoura, T. Pauporté, D. Lincot, T. Oekermann, D. Schlettwein, H. Tada, D. Wöhrle, K. Funabiki, M. Matsui, H. Miura, and H. Yanagi, *Adv. Funct. Mater.*, **19**, 17 (2009).
23. J. A. Parkinson, H. Sun, and P. J. Sadler, *Chem. Commun.*, **8**, 881 (1998).
24. C. L. Kuo, T. J. Kuo, and M. H. Huang, *J. Phys. Chem. B*, **109**, 20115 (2005).
25. S. Cho, J.-W. Jang, S.-H. Jung, B. R. Lee, E. Oh, and K.-H. Lee, *Langmuir*, **25**, 3825 (2009).
26. Z. R. Tian, J. A. Voigt, J. Liu, B. Mckenzie, M. J. Mcdermott, M. A. Rodriguez, H. Konishi, and H. F. Xu, *Nat. Mater.*, **2**, 821 (2003).
27. K. Ichinose, Y. Kimikado, and T. Yoshida, *Electrochem.*, **79**, 146 (2011).
28. T. Pauporté and D. Lincot, *Electrochim. Acta*, **43**, 3345 (2000).
29. Y. Sakuragi, X. Wang, H. Miura, M. Matsui, and T. Yoshida, *J. Photochem. Photobiol. A: Chem.*, **216**, 1 (2010).
30. E. Azaceta, R. Marcilla, D. Mecerreyes, M. Ungureanu, A. Dev, T. Voss, S. Fantini, H.-J. Grande, G. Cabañero, and R. Tena-Zaera, *Phys. Chem. Chem. Phys.*, **13**, 13433 (2011).
31. M. Tulodziecki, J.-M. Tarascon, P. L. Taberna, and C. Guéry, *J. Electrochem. Soc.*, **159**, D691 (2012).
32. E. Azaceta, J. Idigoras, J. Echeberria, A. Zukal, L. Kavan, O. Miguel, H.-J. Grande, J. A. Anta, and R. Tena-Zaera, *J. Mater. Chem. A*, **1**, 10173 (2013).
33. T. Yoshida and H. Minoura, *Adv. Mater.*, **12**, 1219 (2000).
34. O. Lupan, T. Pauporté, L. Chow, B. Viana, F. Pellé, L. K. Ono, B. R. Cueya, and H. Heinrich, *Appl. Surf. Sci.*, **256**, 1895 (2010).
35. T. Voss, C. Bekeny, J. Gutowski, R. Tena-Zaera, J. Elias, C. Lévy-Clément, I. Mora-Seró, and J. Bisquert, *J. Appl. Phys.*, **106**, 054304 (2009).
36. E. Burstein, *Phys. Rev.*, **93**, 632 (1954).
37. T. S. Moss, *Proceedings of the Phys. Soc.*, **67B**, 775 (1954).
38. K. Nonomura, D. Komatsu, T. Yoshida, H. Minoura, and D. Schlettwein, *Phys. Chem. Chem. Phys.*, **9**, 1843 (2007).
39. P. Wanger and R. Helbig, *J. Phys. Chem. Solids*, **35**, 327 (1974).